Article

Tofacitinib is a mechanism-based inactivator of cytochrome P450 3A4

Xiucai Guo, Wei Li, Qingmei Li, Yan Chen, Guode Zhao, Ying Peng, and Jiang Zheng

Chem. Res. Toxicol., **Just Accepted Manuscript** • DOI: 10.1021/acs.chemrestox.9b00141 • Publication Date (Web): 15 Aug 2019

Tofacitinib is a mechanism-based inactivator of cytochrome P450 3A4

Xiucai Guo[†], Wei Li[†], Qingmei Li[†], Yan Chen[†], Guode Zhao[‡], Ying Peng[*, †] and Jiang Zheng[*, †, §]

[†]Wuya College of Innovation, [‡]School of Pharmaceutical Engineering, Shenyang Pharmaceutical University, Shenyang, Liaoning, 110016, P.R. China;

[§]State Key Laboratory of Functions and Applications of Medicinal Plants, Key Laboratory of Pharmaceutics of Guizhou Province, Guizhou Medical University, Guiyang, Guizhou, 550004, P. R. China

Correspondence authors:

Jiang Zheng, Ph.D.

1. Wuya College of Innovation, Shenyang Pharmaceutical University, Shenyang, Liaoning, 110016, P. R. China;

2. State Key Laboratory of Functions and Applications of Medicinal Plants, Key Laboratory of Pharmaceutics of Guizhou Province, Guizhou Medical University, Guiyang, Guizhou, 550004, P. R. China.

The two corresponding units contributed equally to this work.

Email: zhengneu@yahoo.com

Tel: +86-24-23986361 Fax: +86-24-23986510

Ying Peng, Ph.D.

Wuya College of Innovation, Shenyang Pharmaceutical University, PO Box 21,103 Wenhua Road, Shenyang 110016, P. R. China

Email: yingpeng1999@163.com

Tel: +86-24-23986361 Fax: +86-24-23986510

Table of content (TOC) graphic

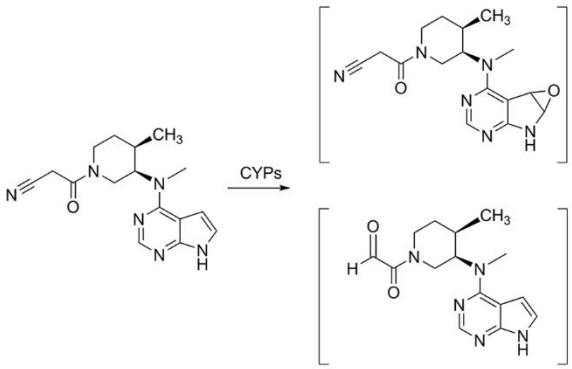

Abstract

Tofacitinib (TFT) is an oral JAK inhibitor which has been approved for the treatment of moderately and severely active rheumatoid arthritis. TFT was found to show concentration-, time- and NADPH-dependent inhibition of CYP3A4, and irreversibility of the inactivation was also observed. Incubation (40 min, 37 °C) of recombinant CYP3A4 with TFT at 200 μM resulted in >70 % loss of CYP3A4 activity. Estimated k_{inact} and K_I were 0.037 min^{-1} and 93.2 μM, respectively. GSH and superoxide dismutase/catalase revealed minor or little protection against the CYP3A4 inactivation. Furthermore, ketoconazole attenuated TFT-mediated CYP3A4 inactivation. Epoxide and α-keto-aldehyde intermediates of TFT were trapped and characterized in microsomal incubations, respectively. The aldehyde intermediate is believed to be the key for the enzyme inactivation. Multiple P450 enzymes, including CYPs2C19, 3A4, 2D6, and 1A2, participated in the metabolism of TFT to the epoxide, while the formation of the aldehyde was mainly catalyzed by CYP3A4. In conclusion, TFT was proven to be a mechanism-based inactivator of CYP3A4.

Introduction

Cytochrome P450 enzymes are a family of heme proteins involved in the metabolism of exogenous and endogenous compounds.[1-2] Pharmaceutical agents are one of the major categories of substrates. Among various drug-metabolizing P450 enzymes, CYP3A4 plays a critical role in the metabolism of marketed drugs up to 50%, and the enzyme shows high-levels of protein expression in small intestine and liver.[1-2] Mechanism-based inactivation (MBI) of P450s remains an important issue in drug discovery and development. MBI provides the potential to amplify the effects of drug-drug interactions by altering drug clearance after other drugs are co-administered and finally results in safety issues during drug use.[3-5]

Tofacitinib (TFT), an oral JAK inhibitor, was approved by the US Food and Drug Administration for the treatment of moderately to severely active rheumatoid arthritis in adult populations.[6] TFT is an inhibitor of JAK1, JAK2, and JAK3, and slightly decreases the activity of tyrosine kinase 2. In a cellular environment, TFT inhibits signaling preferentially by heterodimeric receptors associated with JAK1 and/or JAK3.[6] By inhibition of JAK1 and/or JAK3, TFT is able to block signaling through the receptors containing a common gamma chain for some cytokines, such as interleukin-2, -4, -7, -9, -15, and -21, which are essential for lymphocyte proliferation, activation, and function.[6] Therefore, modulation of multiple aspects of the immune response may be caused by the inhibition of cytokines. In the clinic, TFT is widely used to treat many diseases such as psoriasis[7], rheumatoid arthritis[8-9], and inflammatory bowel disease[10]. Meanwhile, many clinical side effects have been reported, such as headache,

nasopharyngitis, nausea, elevated transaminases, leukopenia, neutropenia, and lymphopenia.[9, 11-13] However, the mechanistic basis of the side effects induced by TFT, especially liver injury, are unclear.

The major metabolic pathways of TFT include glucuronidation, oxidation of the side-chain of the piperidine ring, *N*-demethylation, oxidation of the pyrrolopyrimidine and piperidine rings.[14] Although phase I metabolism of TFT has been well studied, it is far from clear for phase II metabolism of TFT, and the correlation between metabolism and the adverse effects of TFT remains unknown. In the present work, we investigated the metabolic activation of TFT by trapping reactive metabolites generated in microsomal incubations. On the basis of enzyme kinetics, we established that mechanism-based inactivation of CYP3A4 is induced by TFT. These findings provide new understanding of mechanisms of TFT toxic action needed to inform clinical applications.

Materials and methods

Materials and reagents. Tofacitinib (TFT, >98%) was purchased from Dalian Meilun Biotechnology Co., Ltd. (Dalian, China). Human recombinant P450 enzymes were acquired from BD Gentest (Woburn, MA). Nicotinamide adenine dinucleotide phosphate (NADPH), ketoconazole (KTZ), glutathione (GSH), *S*-hexylglutathione, *N*-acetyl-L-cysteine (NAC), testosterone, ammonium acetate, *Nα*-acetyl-L-lysine (NAL), superoxide dismutase (SOD) and catalase from bovine liver were obtained from Sigma-Aldrich Chemical (St. Louis, MO). Mixed male human liver microsomes (HLMs) of Mongolia people were purchased from Research Institute for Liver Diseases (Shanghai) Co., Ltd. (Shanghai, China). Dialysis membrane (cut off: 3,500 Da) was acquired from Beyotime Biotechnology (Shanghai, China). 1-Hydroxybenzotriazole monohydrate (HOBt), di-*tert*-butyl dicarbonate (Boc_2O), propranolol, *β*-alanin, cyanoacetic acid, *N*-(3-dimethylaminopropyl)-*N′*-ethylcarbodiimide hydrochloride (EDCI), and Raney nickel (< 150μM) were obtained from Aladdin Technology (Shanghai, China). *N*-Methyl-*N*-((3R,4R)-4-methylpiperidin-3-yl)-7*H*-pyrrolo[2,3-d]pyrimidin-4-amine hydrochloride (**1** in Scheme 1) was purchased from J & K Scientific Ltd. (Beijing, China). Distilled water was purchased from Wahaha Co. Ltd. (Hangzhou, China). All the other reagents and chemicals were either analytical or high-performance LC grade obtained from various sources.

CYP3A4 assay. The formation of 6*β*-hydroxyl testosterone from testosterone was measured to monitor CYP3A4 activity by LC-MS/MS. Mass spectrometric analysis was performed on an AB SCIEX TRIPLE QUAD^{TM} 5500 (Applied Biosystems, Foster

City, CA) coupled with an LC system (Agilent 1260). A Symmetry C18 column (3.5 μm, 4.6×75 mm; Waters, Wexford, Ireland) was applied for chromatographic separation at 25 °C. Mobile phases were composed of 0.1% (v/v) formic acid in acetonitrile (solvent A) and in water (solvent B). The flow rate was set at 0.8 mL·min^{-1}. A gradient was employed as follows: 20-20% A for 0-1.0 min, 20%-55% A for 1.0-6.5 min, 55-90% A for 6.5-7.0 min, 90-90% for 7.0-8.0 min, 90-20% A for 8.0-8.5 min, and 20-20% for 8.5-10.5 min. Quantification was carried out with multiple reaction monitoring (MRM) for the detection of both internal standard propranolol (*m/z* 260.1→116.1, CE 25) and 6*β*-hydroxyl testosterone (*m/z* 305.2→269.2, CE 21) in positive ion modes.

Determination of concentration-, time-, and NADPH-dependent inactivation of CYP3A by TFT. The primary incubation mixtures consisted of $MgCl_2$ (3.2 mM), HLMs (0.5 mg protein·mL^{-1}), and TFT at various concentrations (0, 25, 50, 75, 100, and 200 μM) with total volume 0.2 mL in 0.1 M potassium phosphate buffer (PBS, pH 7.4). After pre-incubation for 3 min at 37 °C, the primary incubations were triggered by adding NADPH (1.0 mM). In addition, similar incubations without NADPH were carried out as a negative control to investigate the contribution of metabolism on TFT-induced enzyme inhibition. Subsequently, at time points of 0, 10, 20, and 40 min of the incubations, respectively, aliquots (40 μL) of the incubation mixtures were transferred into the secondary incubation mixtures containing NADPH (1.0 mM), $MgCl_2$ (3.2 mM), and testosterone (200 μM) with a total reaction volume of 0.12 mL in 0.1 M PBS (pH 7.4). After that, further reactions (37 °C, 15 min) were performed to assess the

remaining CYP3A activity, and then the reactions were terminated by mixing with ice-cold acetonitrile (equal volume) containing propranolol (internal standard). The resulting mixtures were subjected to centrifugation at 19,000 *g* for 10 min, and the resulting supernatants were analyzed by LC-MS/MS for the assessment of 6*β*-hydroxyl testosterone. To determine whether CYP3A4 or CYP3A5 was inactivated, TFT was incubated with individual human recombinant CYP3A4 and CYP3A5 (50 nmol) instead of HLMs, and similar time-course enzyme inhibition studies were performed as above.

Determination of competitive inhibitor protection. Ketoconazole was used to explore its protective effect on TFT-produced inactivation of CYP3A. The primary reaction mixtures contained HLMs (0.5 mg protein·mL^{-1}), TFT (100 μM), NADPH (1.0 mM), and ketoconazole at various concentrations (0.005, 0.01, and 0.05 μM), and aliquots (40 μL) of the mixtures were taken to determine the remaining testosterone 6*β*-hydroxylase activities at 0, 10, 20, and 40 min post incubations. As control, in parallel, incubations were operated without TFT or ketoconazole.

Determination of effects of GSH and catalase/SOD on TFT-induced enzyme inactivation. With GSH added, the primary incubation mixtures containing TFT (100 μM), NADPH (1.0 mM) and HLMs (0.5 mg protein·mL^{-1}) were incubated at 37 °C. Aliquots (40 μL) were withdrawn for the remaining CYP3A activity determination at various time points. In a separate study, incubations containing TFT, NADPH, and HLMs were performed in the present or absence of catalase (800 unit/mL) and SOD

(800 unit/mL). As control samples, equal volume of PBS (0.1 mM, pH 7.4) was included, instead of GSH or catalase/SOD solution. After incubation at various time point, the remaining testosterone 6β-hydroxylase activities were then assessed as described above.

Determination of irreversibility of inhibition. Incubations containing $MgCl_2$ (3.2 mM), TFT (100 μM), and HLMs (0.5 mg protein·mL^{-1}) were performed with NADPH (1.0 mM) added to trigger the reactions at 37 °C. TFT was absent in control incubations. After incubation for 0 and 40 min, 40 μL of the incubation mixtures were withdrawn in triplicate for enzymatic activity determination. At the same time, equal volume of the incubation mixtures with/without TFT were respectively transferred into dialysis bags and dialyzed against 1 L PBS (0.1 mM) for three times (2 h for each) at 4 °C. The samples obtained from dialysis were allowed to stand to room temperature, followed by determining the residual enzyme activities as described above.

Chemical Synthesis of TFT Analogs. The pyrroline and amino analogs of TFT (**2** and **3** in Scheme 1) were synthesized, according to published literature with modification.[15-16] To synthesize analog **2**, starting material **1** (150 mg, 0.61 mmol) was dissolved in methanol (10 mL), and Raney nickel (20 mg) was then added to catalyze the reaction. The resultant mixture was placed into a sealed and hydrogen-purged reactor and stirred with pressure 5 MPa at 45 °C for 3 days. Sample obtained was filtered and condensed under vacuum, dissolved in CH_2Cl_2 (20 mL), and mixed with triethylamine (2 mL), EDCI·HCl (1.22 mmoL), and HOBt (1.22 mmol). The resulting mixture was stirred at

room temperature for 30 min, followed by addition of cyanoacetic acid (1.22 mmol) and stirring for another 10 h at room temperature. After reaction completion monitored by TLC (ethyl acetate: methanol = 9:1), the mixture was washed with water (10 mL) for three times. The organic layer was collected, dried over anhydrous Na_2SO_4, and concentrated under reduced pressure. Purification of the product was achieved by silica gel chromatography and semi-preparative HPLC. Product **2** (purity >98%) was characterized by MS/MS (Figure S1), Q-TOF MS (Figure S4), and ^{1}H NMR/^{13}C NMR (Figure S2) as shown in supporting information. The synthetic route of analog **2** is shown in Scheme S1.

To synthesize analog **3**, a stirred solution of *β*-alanine (2.0 g, 22.5 mmol) in 10% NaOH (30 mL) over ice-water bath was slowly mixed with 1.2 equiv. of Boc_2O (6 mL, 26.0 mmol) in 20 min. The resulting mixture was kept at room temperature and stirred for 14 h. The resulting mixture was washed with CH_2Cl_2. The aqueous layer was acidified to pH 2~3 with 1.0 M H_2SO_4 and extracted with CH_2Cl_2. The extracts were pooled, dried over anhydrous $NaSO_4$, and concentrated under reduced pressure. The resulting oil was dissolved in a minimum volume of CH_2Cl_2 and kept stirring with petroleum ether added slowly over ice-water bath. The resulting white solid (3.39 g, **4**) was harvested by filtration. After that, compound **1** (100 mg, 0.41 mmol) was dissolved in CH_2Cl_2 (20 mL), followed by addition of triethylamine (0.8 mL), EDCI·HCl (0.82 mmol), and HOBt (0.82 mmol) and stirring at room temperature for 30 min. The resulting mixture was mixed with compound **4** (154 mg, 0.82 mmol) and stirred for 10 h at room temperature. Upon completion of the reaction as indicated by TLC (petroleum

ether: ethyl acetate = 5:1), the reaction mixture was washed with water (10 mL) for three times. The organic layer was collected, dried over anhydrous Na_2SO_4, and concentrated under reduced pressure. Silica gel chromatography eluted with ethyl acetate was employed to purify the product (**5)**. An ethyl acetate solution saturated with HCl was mixed with a solution of **5** in 2 mL ethyl acetate. After stirred for 2 h, the solvent was removed by filtration to obtain faint yellow powder as chloride salt of analog **3**. The final product (**3**, >98%) was characterized by MS/MS (Figure S1), Q-TOF MS (Figure S4), and ^{1}H NMR/^{13}C NMR (Figure S3) as shown in supporting information. The synthetic route of analog **3** is shown in Scheme S1.

Reactive metabolite trapping by NAL and NAC. Incubation mixtures with a total volume of 0.2 mL contained TFT or **2** or **3** (100 μM), NAL (1.0 mM) or NAC (1.0 mM), and HLMs (0.5 mg protein·mL^{-1}) or individual human recombinant P450 enzymes (including CYPs3A4 2A6, 2C9, 3A5, 2C19, 1A2, 2B6, 2D6 or 2E1; 100 nM for each). The reactions were initiated by addition of NADPH (1.0 mM), and the incubations were executed at 37 °C for 30 min. In negative control incubations, NADPH was excluded. Termination of microsomal reactions was executed by addition of ice-cold acetonitrile (equal volume) containing *S*-hexylglutathione (internal standard), followed by vortexing and centrifugation at 19,000 *g* for 10 min. The resultant supernatants were submitted to LC-MS/MS to seek designed NAC/NAL conjugates. The same column was employed for chromatographic separation as described above. Mobile phases consisted of acetonitrile (solvent A) and water containing 5 mM ammonium acetate (solvent B). The flow rate was set at 0.8 mL·min^{-1},

and gradient elution was applied as follows: 10-10% A for 0-2 min,10-40 % A for 2-5.5 min, 40-90% A for 5.5-7.5 min, 90-90% A for 7.5-8.0 min, 90-10% A for 8.0-8.5 min, and 10-10% A for 8.5-11.0 min. MRM scan mode was used to detect metabolites with *m/z* 474→345 for NAC conjugates, *m/z* 472→272, 488→272, 474→274, 490→274 for NAL conjugates and *m/z* 392.2→263.2 for *S*-hexylglutathione. The collision energy (CE) was set at 50 for NAL conjugates, 35 for NAC conjugates and 20 for *S*-hexylglutathione. MS_2 scan mode was employed at a scan range for product ions from *m/z* 50 to 500 in positive mode. The data were analyzed by analyst software of Applied Biosystems/SCIEX.

Determination of effects of TFT analogs on enzyme inactivation. The primary incubation mixtures consisted of $MgCl_2$ (3.2 mM), CYP3A4 (50 nM), and TFT or **2** or **3** (200 μM) in 0.1 M PBS (pH 7.4) with total volume 0.2 mL. The proportion of organic solvent was kept under 1%. Control incubation was also conducted in the absence of TFT or **2** or **3**. After pre-incubation for 3 min at 37 °C, the primary incubations were triggered by adding NADPH (1.0 mM). And at time points of 0, 10, 20, and 40 min after incubation, the remaining CYP3A4 activities were assessed as above.

Results

Concentration-, Time-, and NADPH-dependent inhibition of CYP3A4 by TFT. Residual CYP3A activity of HLMs exposed to TFT was determined by monitoring the catalytic ability to oxidize testosterone to its 6β-hydroxyl metabolite. A natural logarithm plot of percent residual activity against incubation time was employed.[17] The remaining enzyme activity of HLMs after exposure to TFT at 0 min was defined as 100% for comparing the inactivation effects at various incubation time points and concentrations. As displayed in Figure 1A, the remaining enzymatic activities decreased following the increase of the incubation time and concentrations of TFT applied. After HLMs were incubated with 200 μM TFT for 40 min at 37 °C, about 66% of CYP3A activity was lost. Neither TFT-free nor NADPH-free microsomal incubations showed such enzyme activity loss (Figure 1C). The rates (k_{obs}) of the observed enzyme inactivation were acquired from linear regression analyses of the time- and concentration-dependent inhibition data. To estimate the concentration required for maximal rate constant of inactivation (k_{inact}) and half-maximal inactivation (K_I), a double-reciprocal plot of k_{obs} with TFT concentrations was employed according to a published method [17], and the values of k_{inact} and K_I were found to be 0.037 min^{-1} and 93.2 μM, respectively (Figure 1B). Moreover, recombinant enzyme incubation studies demonstrated that 76.7% of CYP3A4 activity was suppressed after 40 min incubation with TFT (200 μM) at 37 °C (Figure 8), but no such enzyme inactivation was observed with CYP3A5 (data not shown) under the same incubation condition.

Competitive inhibitor protection. Ketoconazole is a competitive inhibitor of CYP3A

enzymes and would suppress the metabolism of TFT by CYP3A in HLM incubations. As a result, ketoconazole revealed protective effect against TFT-induced time-dependent inhibition (Figure 2). With the increase of ketoconazole concentrations (0, 5, 10, and 50 nM) applied in HLM incubations, decrease in TFT-induced (100 μM) testosterone 6*β*-hydroxylase inactivation was observed (47.3±1.2%, 55.8±0.9%, 66.7±6.6%, and 87.3±2.9% in the remaining enzyme activity, respectively).

Effects of GSH and catalase/SOD on the inactivation of CYP3A4. GSH is a nucleophilic agent which can react with electrophilic intermediate(s) released from the active site of host enzymes. After 40 min microsomal incubation at 37 °C, TFT exposure (100 μM) resulted in significant CYP3A activity loss (38.9±7.5% activity remained), and the presence of GSH demonstrated limited protection (49.9±6.5% activity remained) against TFT-induced CYP3A inactivation. Besides, scavengers of reactive oxygen species catalase and SOD showed no protection on the observed inactivation of CYP3A.

Irreversibility of inactivation. Protein dialysis experiments were carried out to determine the reversibility of TFT-induced CYP3A inhibition. The residual enzyme activities were adjusted, according to that of control at time 0 min. As a result, compared with those samples without dialysis disposition, there were no marked recoveries of enzyme activities in samples with dialysis (Table 1).

Identification of reactive metabolites. NAC and NAL were used as nucleophilic agents to trap potential reactive intermediates of TFT in microsomal incubations

containing TFT and NADPH. By MRM transition of *m/z* 474→345, three major NAC conjugates were detected at retention time of 5.50 min for M1, 5.75 min for M2, and 6.25 min for M3 (Figure 3B). In comparison, no chromatographic peaks responsible for M1-M3 were observed in NADPH-free microsomal incubations (Figure 3A), which suggests that metabolism was involved in the formation of the three NAC conjugates. The MS result showed that all three compounds displayed $[M+H]^+$ ions at *m/z* 474. Additionally, M1 showed fragment ions at *m/z* 474, 432, 369, 345, 310, 278, 244, 181, 165, and 98 (Figure 3C), M2 revealed ions at *m/z* 474, 432, 369, 345, 310, 278, 181, 165, and 98 (Figure 3D), and M3 displayed fragment ions of *m/z* 474, 345, 310, 272, 246, 181, and 165 (Figure 3E). The product ion at *m/z* 345 as shown in the spectra arises from the indicative and characteristic neutral loss of 129 Da of NAC conjugates, and ions *m/z* 165 and 310 were postulated to be derived from the fragment by the cleavage of the tertiary C-N bond, which indicates that the three compounds were formed by NAC conjugation with moiety 7*H*-pyrrolo[2,3-d]pyrimidine. Furthermore, no such NAC conjugates were detected in analog **2**-fortified incubations in the presence of NAC under the same condition by monitoring the transition of *m/z* 476→347 (data not shown).

In addition, by MRM of the transitions of *m*/*z* 472→272 and 488→272, two NAL conjugates were detected at retention time of 6.09 min for M4 and 6.46 min for M5 (Figure 4B and 4E). No such chromatographic peaks were observed in microsomal incubations without NADPH (Figure 4A and 4D). Likewise, the generation of the NAL conjugates also required P450-mediated metabolism. The MS/MS spectrum of M4 showed fragment ions of *m/z* 488, 444, 400, 383, 272, 246, 235, 173, and 149 (Figure

4C), and the spectrum of M5 displayed product ions of *m/z* 472, 430, 384, 272, 246, 173, and 149 (Figure 4F). The product ion at *m/z* 272 corresponded to the fragment from cleavage of the C-carbonyl bond, and ion *m/z* 149 detected was postulated to be derived from the fragment by the cleavage of the tertiary carbon-N bond of TFT, which indicates that the carbonyl group on the right side of TFT was intact. Moreover, by scanning the *m/z* 402→149 transition, an aldehyde intermediate derived from TFT was detected at retention time of 6.69 min, which was found to require P450-mediated metabolism (Figure 7A and 7B). In addition, in NAL-fortified microsomal incubations with analog **3** under the same condition, no such NAL conjugates were detected by acquiring ion pairs *m/z* 472→272 and 488→272 (data not shown). Instead, two NAL conjugations, as expected, were detected in incubations of analog **2** with NAL by monitoring ion pairs *m/z* 474→274 and 490→274, and the saturation of pyrrolic moiety did not block the formation of the electrophilic center which reacted with NAL (Figure 5).

P450 enzymes responsible for TFT bioactivation. To determine the catalytic efficiency of various P450 enzymes for the metabolic activation of TFT, nine individual human recombinant P450 enzymes (including CYPs3A4 2A6, 2C9, 3A5, 2C19, 1A2, 2B6, 2D6 and 2E1; 100 nM for each) were incubated with TFT in the presence of NAC or NAL, follow by LC-MS/MS analysis. As shown in the Figure 6, the three TFT-NAC conjugates were detected in incubation mixtures containing CYPs2C19, 3A4, 1A2, or 2D6, but the other P450 enzymes examined only played limited roles in the formation of the reactive metabolite trapped by NAC. Differently, it appears that CYP3A4

dominantly catalyzed the generation of the reactive metabolite trapped by NAL, and the other P450 enzymes tested showed limited capabilities of the TFT bioactivation. As expected, the aldehyde intermediate was formed by the catalysis of CYP3A4, and the resulting aldehyde was captured by NAL to form M4 and M5 (Figure 7C).

Effects of TFT analogs on CYP3A4 inactivation. To define the mechanisms of TFT-induced CYP3A4 inactivation, analogs **2** and **3** were synthesized to probe the roles of pyrrole and nitrile moieties in the inactivation induced by TFT. Analog **2** resulted in significant inactivation after 40 min at 37 °C, although the inactivation was not as potent as that of TFT (43.9 ± 4.8% *vs*. 23.3 ± 4.1% in the remaining enzyme activity), while analog **3** barely inactivated CYP3A4 (Figure 8).

Discussion

Our present studies clearly demonstrated that TFT inhibits CYP3A in both concentration- and time-dependent manners (Figure 1), with a k_{inact} of 0.037 min^{-1} and a K_I of 93.2 μM. NADPH was indispensable for TFT-induced CYP3A inactivation, which indicates that the observed enzyme inactivation was mediated by P450 enzymes. Ketoconazole, a competitive CYP3A inhibitor, attenuated TFT-induced CYP3A inactivation in a concentration-dependent manner (Figure 2), indicating that ketoconazole and TFT competed with each other to enter the active site of CYP3A, leading to the observed protective effect. Catalase and SOD, scavengers of reactive oxygen species, failed to protect against enzyme inactivation, which allows us to exclude the involvement of reactive oxygen species potentially formed in the enzymatic reaction.[18]

Mechanism-based enzyme inactivation is considered to result from covalent modification of host enzymes. Exhaustive dialysis did not restore TFT-induced CYP3A inhibition (Table 1), implying that covalent modification was involved in the enzyme inactivation. In addition, the nucleophilic agent GSH exhibited limited ability to attenuate TFT-induced CYP3A inactivation, indicating that reactive metabolites released from the active site of the host enzyme did not induce the enzyme inactivation, even though they reacted with nucleophilic amino acid residues (non-active site). Interestingly, CYP3A5, unlike CYP3A4, was not susceptible to time-dependent inhibition mediated by TFT, since CYP3A5 almost failed to catalyze the oxidation of TFT to the reactive metabolites. Taken together, the evidence indicates TFT is a

mechanism-based inactivator of CYP3A4.

Characterization of reactive metabolites is an important part of mechanism-based enzyme inactivation study. Structurally, TFT contains two potential sites for oxidative metabolism, including pyrrole and cyanomethyl groups, which could be metabolized to pyrrole-epoxide and aldehyde intermediates, respectively. Both of the two intermediates are chemically reactive to nucleophiles, and may cause enzyme inhibition and reported liver injury.[19-20] Pyrrole-epoxide **6** and aldehyde **7** (Scheme 2) were postulated to be the reactive intermediates responsible for covalent modification. NAC and NAL were used as nucleophiles to trap the two intermediates on account of their chemical properties. Three NAC conjugates derived from TFT were detected in NAC-fortified microsomal incubations. Thiols are known to be reactive to epoxides. It is most likely that NAC conjugate formation arose from reaction of NAC with the epoxide, followed by dehydration. Analog **2** was synthesized to probe the role of metabolic epoxidation in bioactivation of TFT. As expected, NAC-fortified microsomal incubation of analog **2** failed to generate the corresponding NAC conjugates, which implies that the double bond of the pyrrole moiety in TFT was required for the formation of the NAC conjugates, and the loss of the unsatuation made the metabolic epoxidation impossible. Interestingly, analog **2** was also found to inactivate CYP3A4 enzyme. In other words, the selective saturation of the double bond did not knock out the inhibitory effect. This indicates that the epoxidation of TFT was not critical for the observed CYP3A4 inactivation (Scheme 2).

In addition, two NAL conjugates were detected in NAL-fortified microsomal

incubations. The MS/MS spectra of the two metabolites displayed the core frame of TFT but without the nitrile group. We speculated that the loss of nitrile resulted from oxidative denitrilation (Scheme 2) and the resulting α-keto-aldehyde reacted with the trapping agent to form the two NAL conjugates. Metabolic activation of analog **3**, a product resulting from nitrile reduction of TFT, was investigated, and no such NAL conjugates were detected in microsomal incubations. It is not surprising since analog **3** is unable to undergo oxidative denitrilation. Furthermore, analog **3** did not induce CYP3A4 inactivation at all (Figure 8), which suggests that the oxidative denitrilation was essential for TFT-induced CYP3A4 inactivation (Scheme 2). Additionally, two analog **2**-derived NAL conjugates were detected (Figure 5) in NAL-fortified microsomal incubations after exposure to analog **2**. This could explain why analog **2** remained the ability to inactivate CYP3A4 (Figure 8). This may also support the proposed mechanism that oxidative denitrilation of TFT offered α-keto-aldehyde **7** that reacted with apoprotein or/and heme resulting in enzyme inactivation (Scheme 2). Furthermore, it appears that the formation of the NAL-conjugates and α-keto-aldehyde was mediated by CYP3A4 rather than CYP3A5, which could explain why TFT failed to inhibit CYP3A5 activity.

Mechanism-based inactivation of drug-metabolizing enzymes could lead to severe drug-drug interactions when other drugs are co-administered. Toxic and side effects could be caused by resulting elevated plasma levels of the drug, increasing internal exposure. Examples like this often occur: Paroxetine (a mechanism-based inactivator of CYP2D6) co-administrated in patients with risperidone medication for schizophrenia

or schizoaffective disorder caused 1.5-fold elevation of concentrations of risperidone;[21-22] Oral midazolam in healthy volunteers pretreated with verapamil (a mechanism-based inactivator of CYP3A4) showed three times AUC elevation and the peak concentration of midazolam was doubled compared with that pretreatment with placebo;[23-24] Imatinib (a mechanism-based inactivator of CYP3A4) significantly decreased the total-body clearance of drug from plasma with a mean reduction of 70% for simvastatin.[25-26] In the present work, TFT was proven to be a mechanism-based inactivator of CYP3A4, suggesting caution for the application of TFT, especially co-administrated with other medicines, to avoid the likelihood of adverse drug-drug interactions.

Metabolic activation of drugs is an important mechanism for drug-induced liver injury, and reactive metabolites could react irreversibly with endogenous macromolecules, which may result in the alternation of physiological function.[27] The discovery of the two reactive metabolites provides a potential biochemical basis for liver damage induced by TFT, and suggests that further research is needed to determine their contributions to TFT-induced liver injury.

In conclusion, strong evidence indicates that TFT acted as a mechanism-based inactivator of CYP3A4 in a time- and concentration-dependent manner, and the inhibition of CYP3A4 was irreversible. TFT was metabolized by HLMs and human recombinant P450 enzymes to electrophilic pyrrole-epoxide and α-keto-aldehyde intermediates, and the latter may be responsible for the observed CYP3A4 inactivation.

Supporting Information. [Additional figures and experimental procedures.]

Abbreviations:

TFT, tofacitinib; RSD, relative standard deviation; IS, internal standard; ESI, electrospray ionization source; KTZ, ketoconazole; NAC, *N*-Acetyl-L-cysteine; EP, entrance potential; MRM, multiple reaction monitoring; GSH, glutathione; DP, declustering potential; NAL, *Nα*-Acetyl-L-lysine; CE, collision energy; NADPH, nicotinamide adenine dinucleotide phosphate; CXP, collision cell exit potential; HOBt, 1-Hydroxybenzotriazole Monohydrate; SOD, superoxide dismutase; EDCI, *N*-(3-Dimethylaminopropyl)-*N′*-ethylcarbodiimide hydrochloride; HLMs, human liver microsomes; Boc_2O, Di-*tert*-butyl dicarbonate; PBS, potassium phosphate buffer; AUC, area under the concentration-time curve.

Funding sources

This work was supported in part by the National Natural Science Foundation of China (Grants 81430086, 81773813, 81830104).

Notes

The authors declare no competing financial interest.

Reference

(1) Guengerich, F. P. (2001) Common and uncommon cytochrome P450 reactions related to metabolism and chemical toxicity. *Chem. Res. Toxicol. 14,* 611-650.

(2) Guengerich, F. P. (2003) Cytochromes P450, drugs, and diseases. *Mol. Interv. 3,* 194-204.

(3) Fletcher, C. V., Acosta, E. P., Cheng, H., Haubrich, R., Fischl, M., Raasch, R., Mills, C., Hu, X. J., Katzenstein, D., Remmel, R. P., and Gulick, R. M. (2000) Competing drug-drug interactions among multidrug antiretroviral regimens used in the treatment of HIV-infected subjects: ACTG 884. *AIDS. 14,* 2495-2501.

(4) Fernández-Montero, J. V., Barreiro, P., and Soriano, V. (2009) HIV protease inhibitors: recent clinical trials and recommendations on use. *Expert Opin Pharmacother. 10,* 1615-1629.

(5) Miller, C. D., El-Kholi, R., Faragon, J. J., and Lodise, T. P. (2007) Prevalence and risk factors for clinically significant drug interactions with antiretroviral therapy. *Pharmacotherapy. 27,* 1379-1386.

(6) Meyer, D. M., Jesson, M. I., Li, X., Elrick, M. M., Funckes-Shippy, C. L., Warner, J. D., Gross, C. J., Dowty, M. E., Ramaiah, S. K., Hirsch, J. L., Saabye, M. J., Barks, J. L., Kishore, N., and Morris, D. L. (2010) Anti-inflammatory activity and neutrophil reductions mediated by the JAK1/JAK3 inhibitor, CP-690,550, in rat adjuvant-induced arthritis. *J. Inflamm (Lond). 7,* 41.

(7) Boy, M. G., Wang, C., Wilkinson, B. E., Chow, V. F., Clucas, A. T., Krueger, J. G., Gaweco, A. S., Zwillich, S. H., Changelian, P. S., Chan, G. (2009) Double-blind,

placebo-controlled, dose-escalation study to evaluate the pharmacologic effect of CP-690,550 in patients with psoriasis. *J. Invest. Dermatol. 129,* 2299-2302.

(8) Coombs, J. H., Bloom, B. J., Breedveld, F. C., Fletcher, M. P., Gruben, D., Kremer, J. M., Burgos-Vargas, R., Wilkinson, B., Zerbini, C. A., and Zwillich, S. H. (2010) Improved pain, physical functioning and health status in patients with rheumatoid arthritis treated with CP-690,550, an orally active Janus kinase (JAK) inhibitor: results from a randomized, double-blind, placebo-controlled trial. *Ann. Rheum. Dis. 69,* 413-416.

(9) Kremer, J. M., Bloom, B. J., Breedveld, F. C., Coombs, J. H., Fletcher, M. P., Gruben, D., Krishnaswami, S., Burgos-Vargas, R., Wilkinson, B., Zerbini, C. A., and Zwillich, S. H. (2009) The safety and efficacy of a JAK inhibitor in patients with active rheumatoid arthritis: results of a double-blind, placebo-controlled phase IIa trial of three dose levels of CP-690,550 versus placebo. *Arthritis Rheum. 60,* 1895-1905.

(10) Sandborn, W. J., Ghosh, S., Panes, J., Vranic, I., Su, C., Rousell, S., and Niezychowski, W. (2012) Tofacitinib, an oral Janus kinase inhibitor, in active ulcerative colitis. *N. Engl. J. Med. 367,* 616-624.

(11) Tanaka, Y., Suzuki, M., Nakamura, H., Toyoizumi, S., and Zwillich, S. H. (2011) Phase II study of tofacitinib (CP-690,550) combined with methotrexate in patients with rheumatoid arthritis and an inadequate response to methotrexate. *Arthritis Care Res (Hoboken). 63,* 1150-1158.

(12) He, Y., Wong, A. Y., Chan, E. W., Lau, W. C., Man, K. K., Chui, C. S., Worsley,

A. J., and Wong, I. C. (2013) Efficacy and safety of tofacitinib in the treatment of rheumatoid arthritis: a systematic review and meta-analysis. *BMC Musculoskelet Disord. 14,* 298.

(13) Fleischmann, R., Kremer, J., Tanaka, Y., Gruben, D., Kanik, K., Koncz, T., Krishnaswami, S., Wallenstein, G., Wilkinson, B., Zwillich, S. H., and Keystone, E. (2016) Efficacy and safety of tofacitinib in patients with active rheumatoid arthritis: review of key Phase 2 studies. *Int. J. Rheum. Dis. 19,* 1216-1225.

(14) Dowty, M. E., Lin, J., Ryder, T. F., Wang, W., Walker, G. S., Vaz, A., Chan, G. L., Krishnaswami, S., and Prakash, C. (2014) The pharmacokinetics, metabolism, and clearance mechanisms of tofacitinib, a janus kinas inhibitor, in humans. *Drug Metab. Dispos. 42,* 759-773.

(15) Yang, X., Zhang, L., Chen, Q., Liao, M., Huang, C., and Ding, L. Process for preparation tofacitinib analog compound: CN Patent 104926816 [P]. 2015-09-23.

(16) Mouterde, L. and Stewart, J. (2016) An efficient chemoenzymatic synthesis of coenzyme A and its disulfide. *Org. Process Res. Dev. 20,* 954-959.

(17) Nagar, S., Jones, J. P., and Korzekwa, K. (2014) A numerical method for analysis of in vitro time-dependent inhibition data. Part 1. Theoretical considerations. *Drug Metab. Dispos. 42,* 1575-1586.

(18) Klaassen, C. D., Amdur, M. O., and Doull, J. (1986) Biotransformation of xenobiotics. In: Klaassen CD, ed. Casarett and Doull's Toxicology, the basic science of poisons. New York: McGraw-Hill, 113-186.

(19) Wang, K., Wang, H., Peng, Y., and Zheng, J. (2016) Identification of Epoxide-

Derived Metabolite(s) of Benzbromarone. *Drug Metab. Dispos. 44,* 607-615.

(20) Kamel, A. and Harriman, S. (2013) Inhibition of cytochrome P450 enzymes and biochemical aspects of mechanism-based inactivation (MBI). *Drug Discov. Today. Technol. 10,* e177-e189.

(21) Spina, E., Avenoso, A., Facciolà, G., Scordo, M. G., Ancione, M., and Madia, A. (2001) Plasma concentrations of risperidone and 9-hydroxyrisperidone during combined treatment with paroxetine. *Ther. Drug Monit. 23,* 223-227.

(22) Bertelsen, K. M., Venkatakrishnan, K., Von Moltke, L. L., Obach, R. S., Greenblatt, D. J. (2003) Apparent mechanism-based inhibition of human CYP2D6 in vitro by paroxetine: comparison with fluoxetine and quinidine. *Drug Metab. Dispos. 31,* 289-293

(23) Wang, Y. H., Jones, D. R., Hall, S. D. (2004) Prediction of cytochrome P4503A inhibition by verapamil enantiomers and their metabolites. *Drug Metab. Dispos. 32,* 259-266.

(24) Backman, J. T., Olkkola, K. T., Aranko, K., Himberg, J. J., Neuvonen, P. J. (1994) Dose of midazolam should be reduced during diltiazem and verapamil treatments. *Brit. J. Clin. Pharmacol. 37,* 221-225.

(25) Filppula, A. M., Laitila, J., Neuvonen, P. J., and Backman, J. T. (2012) Potent mechanism-based inhibition of CYP3A4 by imatinib explains its liability to interact with CYP3A4 substrates. *Brit. J. Pharmacol. 165,* 2787-2798.

(26) O'Brien, S. G., Meinhardt, P., Bond, E., Beck, J., Peng, B., Dutreix, C., Mehring, G., Milosavljev, S., Huber, C., Capdeville, R., and Fischer, T. (2003) Effects of

imatinib mesylate (STI571, Glivec) on the pharmacokinetics of simvastatin, a cytochrome P450 3A4 substrate, in patients with chronic myeloid leukaemia. *Brit. J. Cancer 89,* 1855-1859.

(27) Gomez-Lechon, M. J., Tolosa, L., and Donato, M. T. (2016) Metabolic activation and drug-induced liver injury: in vitro approaches for the safety risk assessment of new drugs. *J. Appl. Toxicol. 36,* 752-768.

Table Legends

Table 1. Irreversibility of CYP3A inhibition by TFT. Data represent the mean ± SD (n = 3).

	No dialysis		Dialysis
Pre-incubation	0 min	40 min	40 min
% residual activity			
Vehicle	100±7.4	84.2±3.5	56.3±2.3
TFT	80.1±5.4	25.9±1.9	16.2±2.0
% of control	80.1	30.8	28.8

Figure Legends

Scheme 1. Structure of TFT, *N*-methyl-*N*-((3R,4R)-4-methylpiperidin-3-yl)-7*H*-pyrrolo[2,3-d]pyrimidin-4-amine hydrochloride (**1**), analog **2**, analog **3**, *N*-[(1,1-dimethylethoxy)carbonyl]-*β*-alanine (**4**), and compound **5**.

Scheme 2. Proposed pathways of TFT metabolic activation.

Figure 1. A: Time-course CYP3A activity remaining after exposure to TFT. Primary incubation mixtures consisted of HLMs, NADPH and TFT at concentrations of 0 (■), 25 (●), 50 (▲), 75 (✳), 100 (◆), and 200 (◁) μM, respectively. Remaining enzymatic activities were measured at various time points post incubation. B: Double-reciprocal plot of the rates of the values for k_{obs} versus the concentrations of TFT. The k_{obs} was obtained from the slope of linear equations calculated from above (A). C: NADPH-dependent inhibition of CYP3A by TFT. Incubations consisted of HLMs and vehicle (▲) or TFT (100 μM) in the presence (■) or absence (◆) of NADPH. Data represent the mean ± SD (n = 3).

Figure 2. Competitive inhibitor protection against inactivation of CYP3A by TFT. Incubations consisted of HLMs and vehicle (■) or TFT (100 μM) with (✳, 0.05 μM ; ◆, 0.01 μM; ▲, 0.005 μM) or without (●) ketoconazole. Data represent the mean ± SD (n = 3).

Figure 3. Mass spectrometric chromatograms (ion pair *m/z* 474→345) obtained from LC-MS/MS analysis of incubation mixtures containing HLMs, TFT and NAC with (B) or without (A) NADPH. C: Mass spectral fragment ions of M1 generated in microsomal incubations. D: Fragment ions of M2. E: Fragment ions of M3.

Figure 4. Mass spectrometric chromatograms (ion pair *m/z* 488→272) obtained from LC-MS/MS analysis of incubation mixtures containing HLM, TFT and NAL with (B) or without (A) NADPH. C: Mass spectral fragment ions of M4 generated in microsomal incubation. Mass spectrometric chromatograms (ion pair *m/z* 472→272) obtained from LC-MS/MS analysis of incubations containing HLMs, TFT and NAL with (E) or without (D) NADPH. F: Mass spectral fragment ions of M5 generated in microsomal incubations.

Figure 5. Mass spectrometric chromatograms (ion pair *m/z* 490→274) obtained from LC-MS/MS analysis of incubations mixtures containing HLMs, analog **2**, and NAL with (B) or without (A) NADPH. C: Mass spectral fragment ions of NAL conjugates (*m/z* 490→274) generated in microsomal incubations. Mass spectrometric chromatograms (ion pair *m/z* 474→274) obtained from LC-MS/MS analysis of incubation mixtures containing HLMs, analog **2** and NAL with (E) or without (D) NADPH. F: Mass spectral fragment ions of NAL conjugates (*m/z* 474→274) generated in microsomal incubations.

Figure 6. A: Formation of TFT-derived NAC conjugates in individual recombinant P450 enzyme incubations containing NADPH, TFT, and NAC. B: Formation of TFT-derived NAL conjugates in individual recombinant P450 enzyme incubations containing NADPH, TFT, and NAL. Data represent the mean ± SD (n = 3).

Figure 7. Mass spectrometric chromatograms (ion pair *m/z* 402→149) possibly responsible for aldehyde **7** obtained from LC-MS/MS analysis of incubation mixtures containing HLMs and TFT with (B) or without (A) NADPH. C: Formation of aldehyde

7 in individual recombinant P450 enzyme incubations containing NADPH and TFT. Data represent the mean ± SD (n = 3).

Figure 8. Time-course CYP3A4 activity remaining after exposure to TFT or TFT analogs. Incubations consisted of recombinant CYP3A4, NADPH, along with vehicle (■), TFT (●), analog **3** (▲) or analog **2** (▼) at concentration of 200 μM. CYP3A4 activity was assessed at 0, 10, 20, and 40 min of incubation at 37 °C. The remaining activity at 0 min was calculated as 100% for comparing the inactivation effects of the test compounds. Data represent the mean ± SD (n = 3), $^{**}p < 0.01$ vs. vehicle.

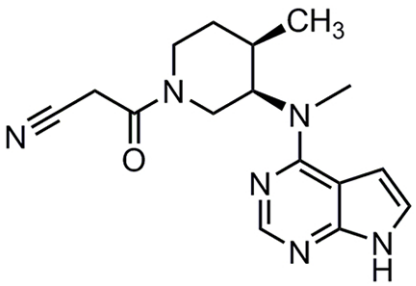

Tofacitinib (TFT)

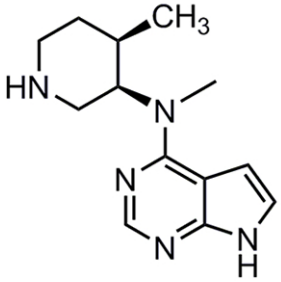

1

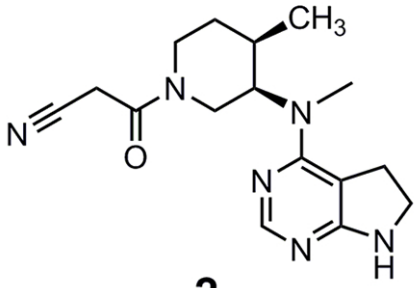

2

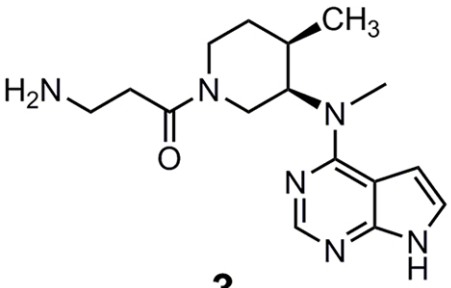

3

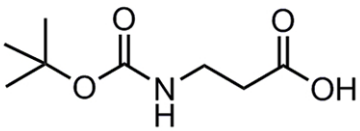

4

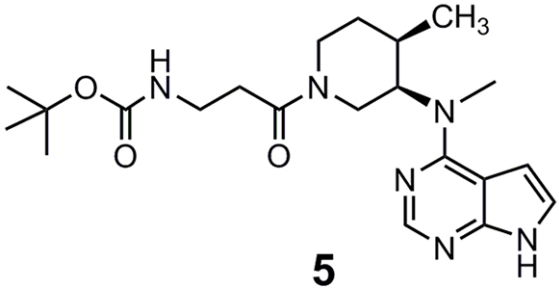

5

Scheme 1.

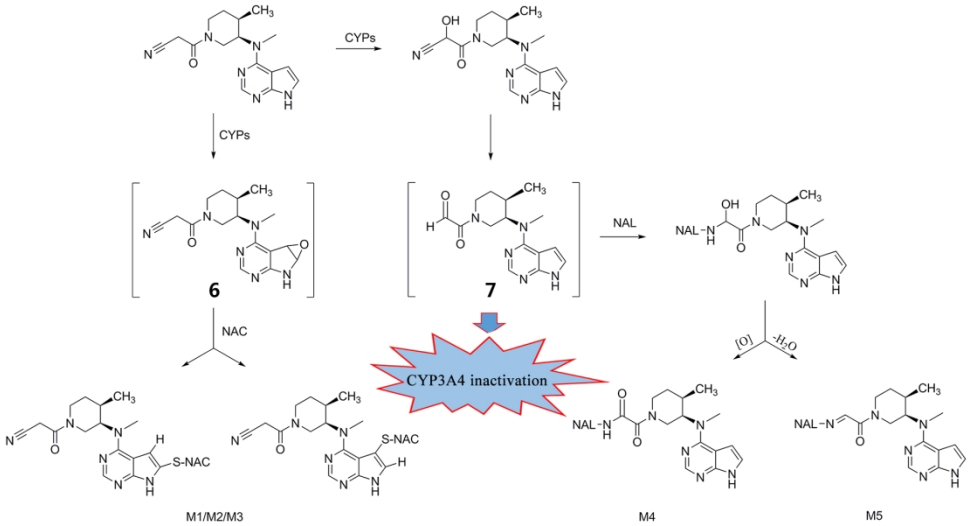
CYPs
CYPs
6
7
NAL
NAC
CYP3A4 inactivation
S-NAC
S-NAC
M1/M2/M3
M4
M5

Scheme 2.

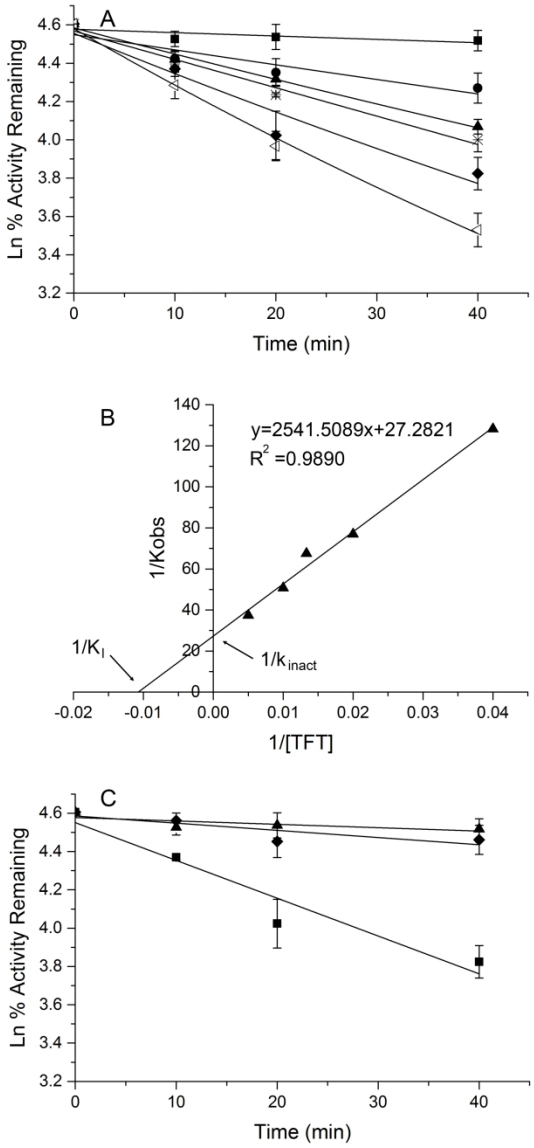

Figure 1.

89x180mm (600 x 600 DPI)

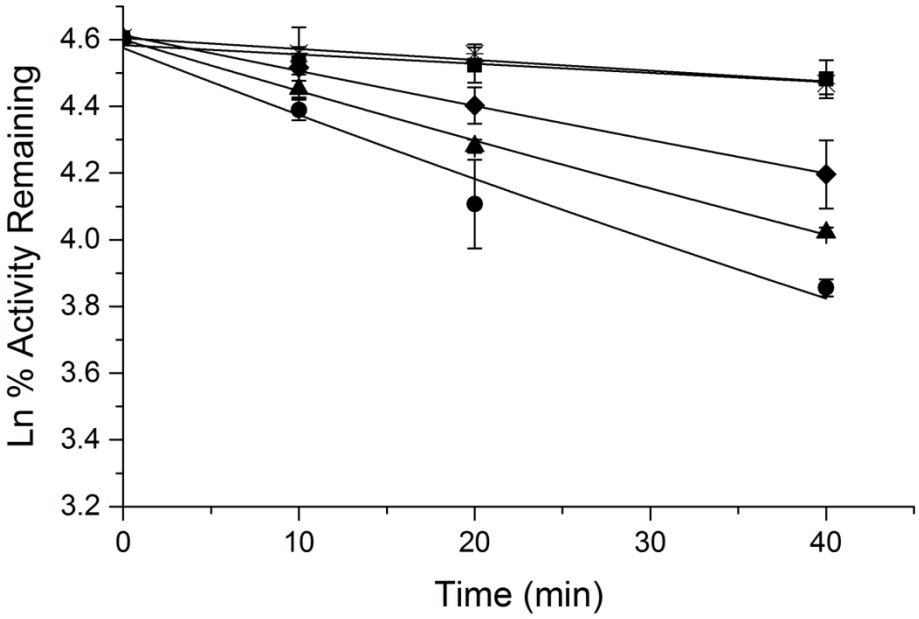

Figure 2.

88x62mm (600 x 600 DPI)

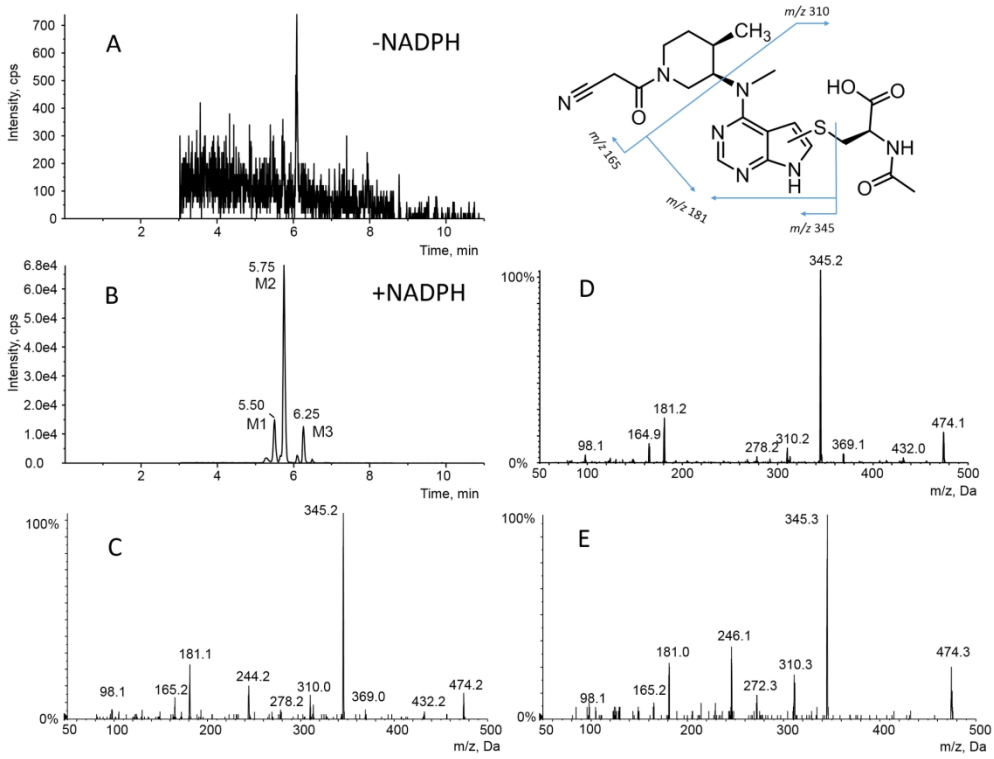

Figure 3.

178x136mm (300 x 300 DPI)

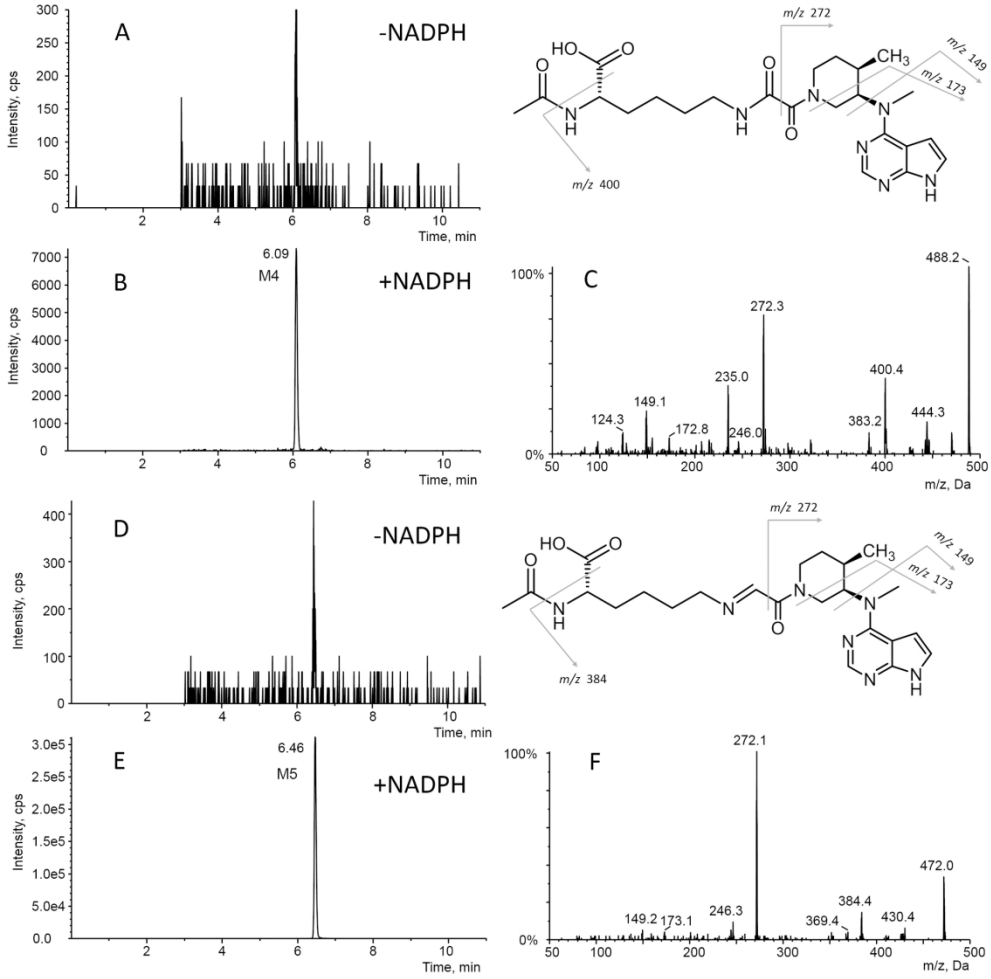

Figure 4.

180x184mm (300 x 300 DPI)

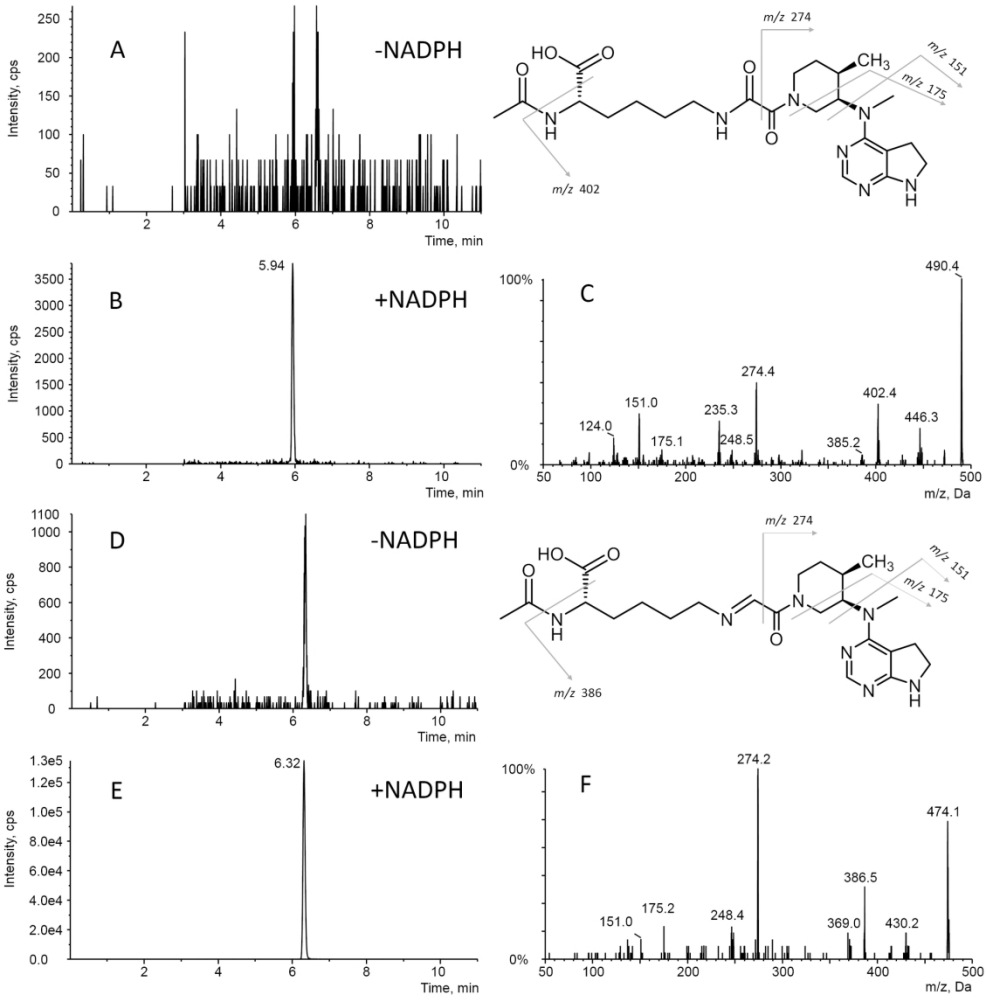

Figure 5.

179x185mm (300 x 300 DPI)

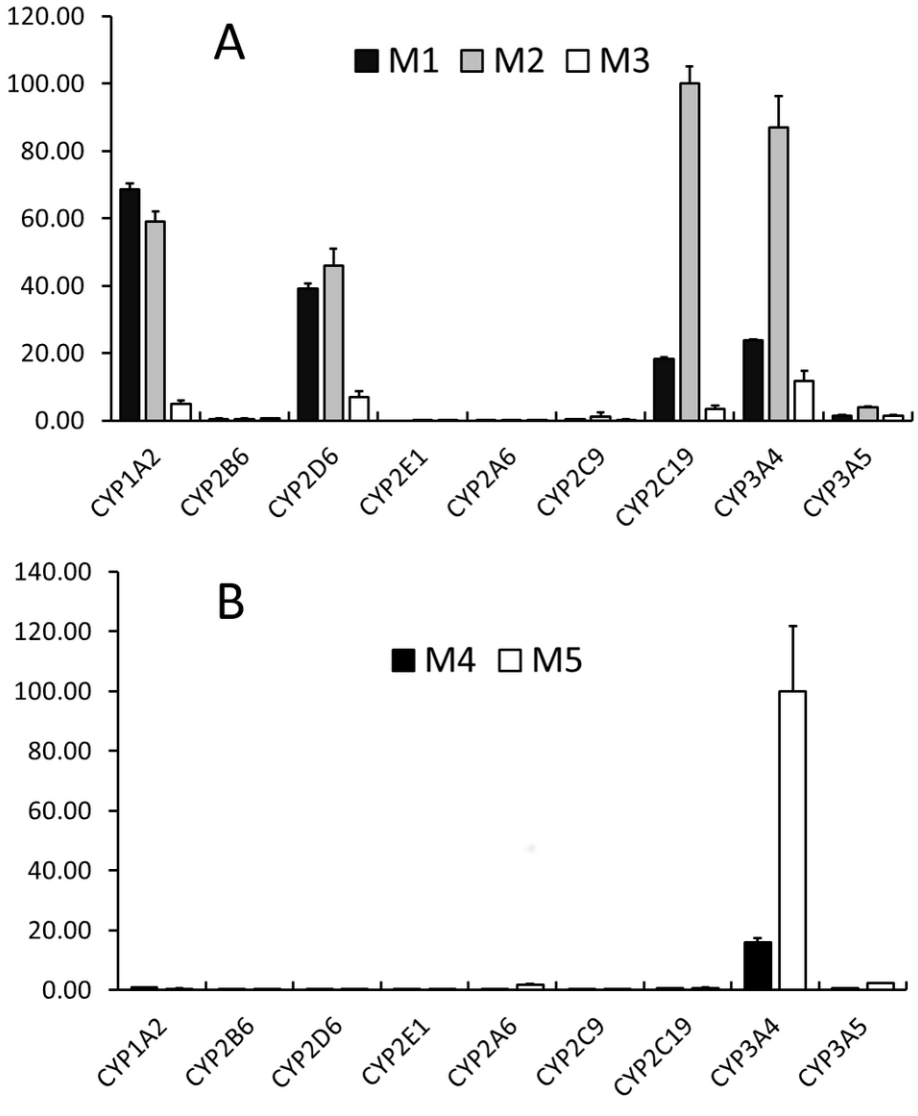

Figure 6.

88x103mm (300 x 300 DPI)

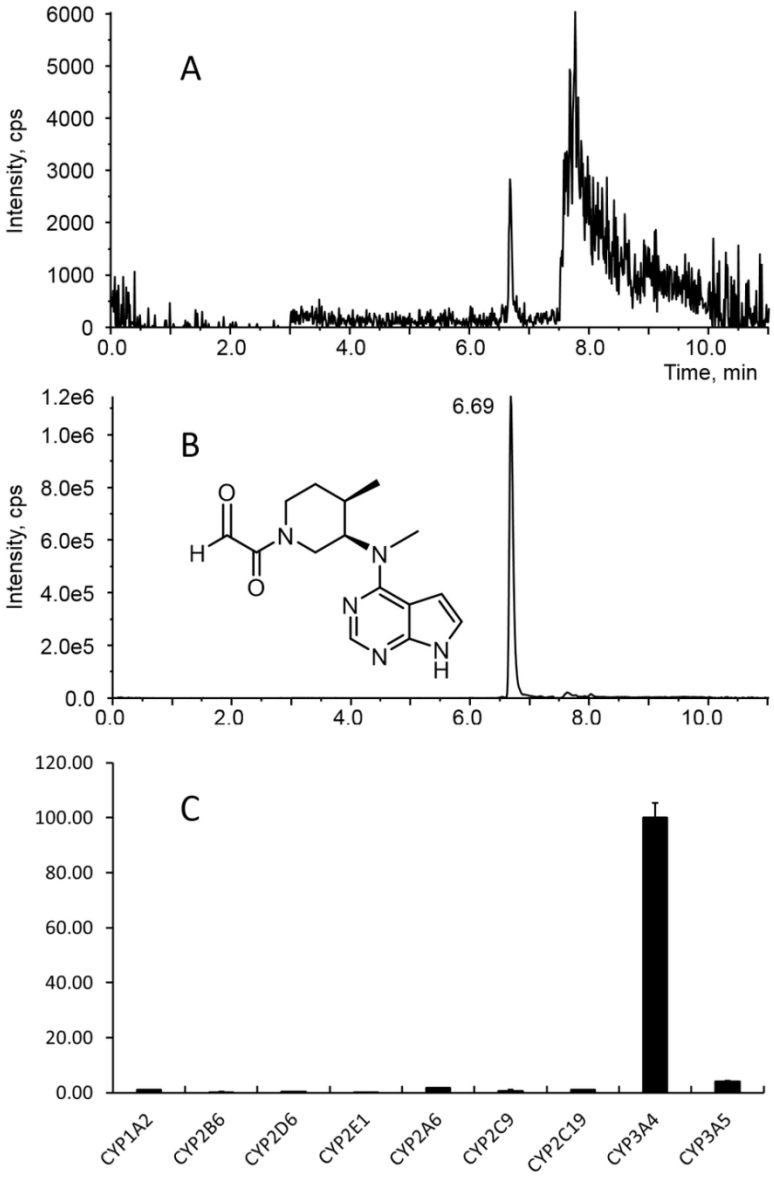

Figure 7.

88x125mm (300 x 300 DPI)

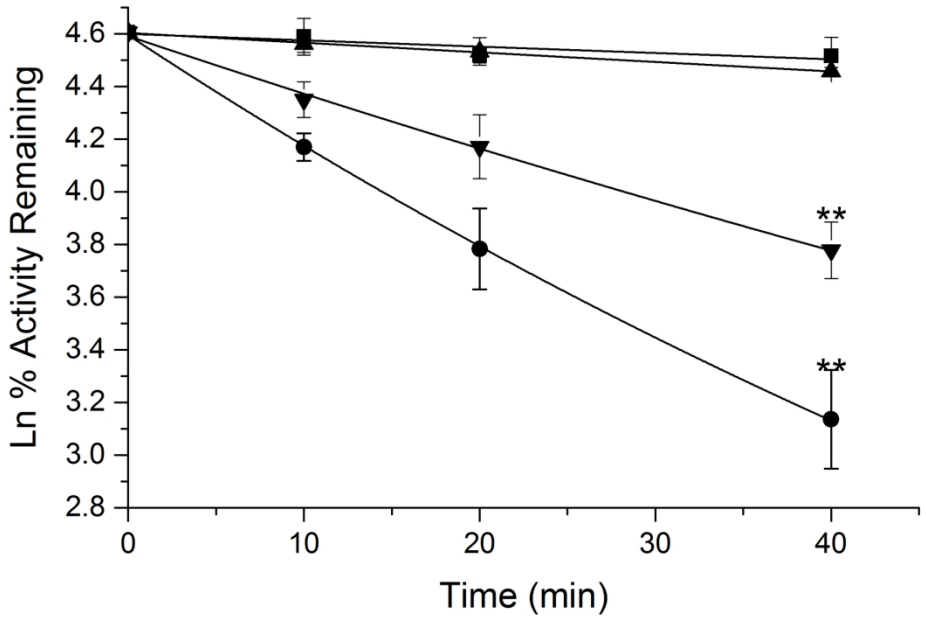

Figure 8.

88x62mm (600 x 600 DPI)